



pubs.acs.org/jacsau Article

Water Triggered Synthesis of Highly Stable and Biocompatible 1D Nanowire, 2D Nanoplatelet, and 3D Nanocube CsPbBr₃ Perovskites for Multicolor Two-Photon Cell Imaging

Avijit Pramanik, Shamily Patibandla, Ye Gao, Kaelin Gates, and Paresh Chandra Ray*



Cite This: JACS Au 2021, 1, 53-65



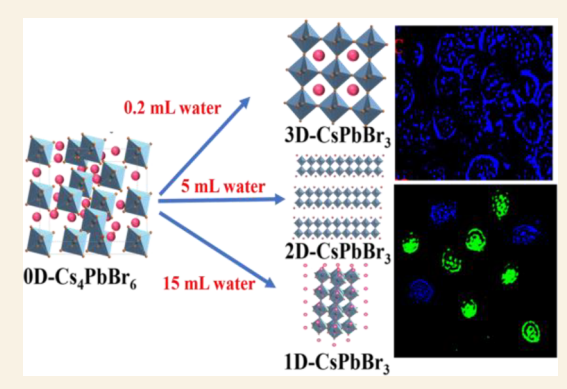
ACCESS

III Metrics & More

Article Recommendations

S Supporting Information

ABSTRACT: Two-photon imaging in the near-infrared window holds huge promise for real life biological imaging due to the increased penetration depth. All-inorganic CsPbX₃ nanocrystals with bright luminescence and broad spectral tunability are excellent smart probes for two-photon bioimaging. But, the poor stability in water is a well-documented issue for limiting their practical use. Herein, we present the development of specific antibody attached water-resistant one-dimensional (1D) CsPbBr₃ nanowires, two-dimensional (2D) CsPbBr₃ nanoplatelets, and three-dimensional (3D) CsPbBr₃ nanocubes which can be used for selective and simultaneous two-photon imaging of heterogeneous breast cancer cells in the near IR biological window. The current manuscript reports the design of excellent photoluminescence quantum yield (PLQY), biocompatible and photostable 1D CsPbBr₃ nanowires, 2D CsPbBr₃ nanoplatelets, and 3D CsPbBr₃ nanocubes



through an interfacial conversion from zero-dimensional (0D) Cs_4PbBr_6 nanocrystals via a water triggered strategy. Reported data show that just by varying the amount of water, one can control the dimension of $CsPbBr_3$ perovskite crystals. Time-dependent transition electron microscopy and emission spectra have been reported to find the possible pathway for the formation of 1D, 2D, and 3D $CsPbBr_3$ nanocrystals from 0D Cs_4PbBr_6 nanocrystals. Biocompatible 1D, 2D, and 3D $CsPbBr_3$ nanocrystals were developed by coating with amine—poly(ethylene glycol)—propionic acid. Experimental data show the water-driven design of 1D, 2D, and 3D $CsPbBr_3$ nanocrystals exhibits strong single-photon PLQY of \sim 66–88% as well as excellent two-photon absorption properties (σ_2) of \sim 8.3 × 10⁵–7.1 × 10⁴ GM. Furthermore, reported data show more than 86% of PL intensity remains for 1D, 2D, and 3D $CsPbBr_3$ nanocrystals after 35 days under water, and they exhibit excellent photostability of keeping 99% PL intensity after 3 h under UV light. The current report demonstrates for the first time that antibody attached 1D and 2D perovskites have capability for simultaneous two-photon imaging of triple negative breast cancer cells and human epidermal growth factor receptor 2 positive breast cancer cells. $CsPbBr_3$ nanocrystals exhibit very high two-photon absorption cross-section and good photostability in water, which are superior to those of commonly used organic probes (σ_2 = 11 GM for fluorescein), and therefore, they have capability to be a better probe for bioimaging applications.

KEYWORDS: water triggered synthesis, 1D, 2D, and 3D CsPbBr₃ nanocrystals, biocompatible CsPbBr₃ perovskites, two photon absorption properties, two photon luminescence imaging of cancer cells, triple negative breast cancer cell identification

1. INTRODUCTION

All-inorganic cesium lead halide (CsPbX₃, X = Cl, Br, and I) perovskites exhibit excellent photoluminescence quantum yield (PLQY), IP luminescence emission, and large two-photon (2P) absorption cross sections, which allow them to be a promising candidate for next-generation bioimaging materials. However, the major obstacle for future bioimaging material applications for perovskites is the poor stability in water due to their ionic nature. As we and others have reported, CsPbX₃ perovskites decompose fast when exposed to water or kept in a moist environment. As a result, enhancing the long-time stability of CsPbX₃ perovskites is the most important parameter to promote commercial applications. $^{30-44}$

As a result, enhancing the long-time stability of $CsPbX_3$ perovskites is the most important parameter to promote commercial applications.^{30–44} In the past few years, there have been enormous efforts to enhance stability of zero-dimensional (0D), one-dimensional (1D), two-dimensional (2D), and

Received: September 29, 2020 Published: December 9, 2020





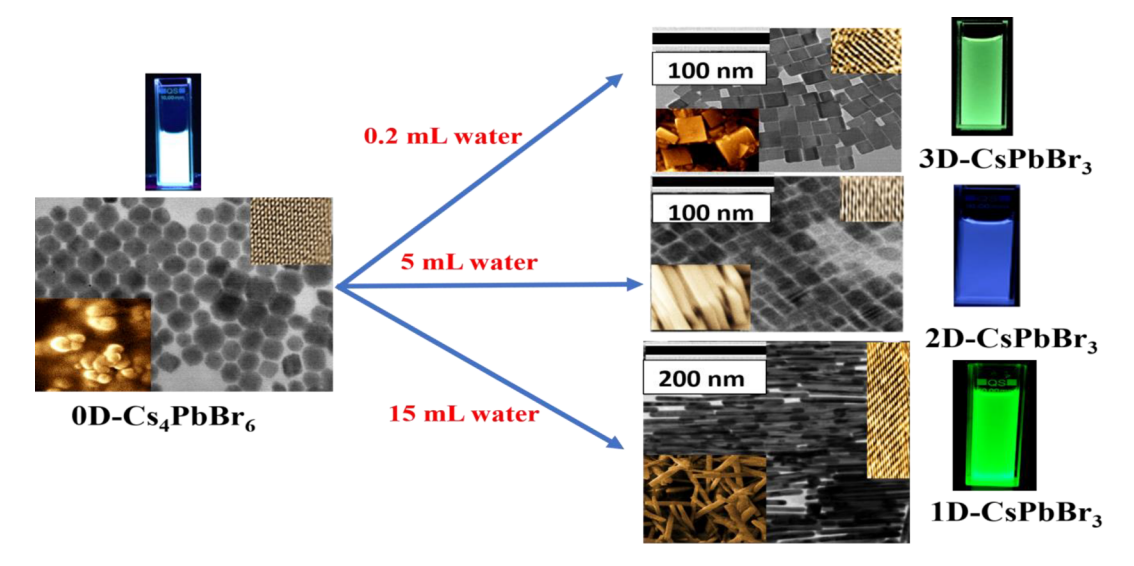


Figure 1. TEM image, inserted HRTEM image, inserted SEM image, and photograph of water resistant 1D, 2D, and 3D CsPbBr $_3$ perovskite nanocrystals derived through an interfacial conversion from 0D Cs $_4$ PbBr $_6$ nanocrystals using different amounts of water.

three-dimensional (3D) lead halide perovskites by functionalizing them with moisture-tolerant molecules.^{34–54}

Despite these great efforts, reports on 1D, 2D, and 3D lead halide perovskite-based two-photon bioimaging is rare. As a result, it is highly desirable to develop a method which can produce water resistant, biocompatible, and photostable 1D, 2D, and 3D perovskite, and these nanocrystals will have capability for two-photon bioimaging applications. As we and others reported, two-photon absorption (2PA) is a nonlinear process where near-infrared light (NIR) in a biological window can be used, which features deep penetration depths, higher spatial resolution, and smaller sample damage for bioimaging and photodynamic therapy. 55-71 Driven by the need, herein, we report the development of high water resistance, excellence photoluminescence quantum yield (PLQY), biocompatible and photostable 1D CsPbBr3 nanowires, 2D CsPbBr3 nanoplatelets, and 3D CsPbBr3 nanocubes through an interfacial conversion from 0D Cs₄PbBr₆ nanocrystals via a water triggered strategy using water and amine-poly(ethylene glycol)-propionic acid (NH₂-PEG₁₂-CH₂-CH₂-CO₂H). As shown in Figure 1, for the design of water-resistant lead halide perovskites, a small amount of water has been used for aqueous phase exfoliation of nonluminescence 0D CsPbBr₃ perovskite to very bright luminescence 1D, 2D, and 3D CsPbBr₃ perovskite. In the ultimate product, water also helps to decorate them with -OH ligands, which allows them to exhibit moisture stability. On the other hand, for the design of biocompatible and photostable lead halide perovskites, a PEG moiety was used, which also acts as a protection layer to effectively prevent degradation of PQDs in water. The same PEG ligand has been used to anchor a biospecific antibody so that perovskites can be used for specific bioimaging applications. Reported data show that 85% IP luminescence and 2PL intensity remains after 3 weeks under water for PEG coated 1D, 2D, and 3D nanocrystals. PEG coated CsPbBr₃ perovskite exhibits excellent photostability of keeping 99% PL intensity after 3 h under UV.

Although breast cancer has been known since 3000 BCE, it is still the second leading cause of cancer deaths in women. ⁵⁵⁻⁶⁸ Because triple negative breast cancer (TNBC) is highly aggressive and lacks an estrogen receptor (ER),

progesterone receptor (PR), and human epidermal growth factor receptor 2 (HER-2), distinguishing TNBC from other types of breast cancers is one of the highest priorities in clinics. As a proof of concept, we demonstrated for the first time that specific antibody attached 1D and 2D perovskites are capable for selective and simultaneous two-photon imaging of TNBC cells and HER-2 positive breast cancer cells. In the two-photon imaging process, CsPbBr₃ perovskites simultaneously absorb two monochromatic infrared photons in the biological window and emit a shorter wavelength photon, which offers significant advantages for bioimaging. SS-68

2. RESULTS AND DISCUSSION

2.1. Water Triggered Synthesis of 3D CsPbBr₃ Nanocubes from 0D Cs₄PbBr₆ Nanocrystals Using 0.2 mL of Water

Initially, we developed 0D Cs₄PbBr₆ NCs using the hot injection method as we and others have reported before 25-40 (see more details in the experimental section in the Supporting Information). The freshly prepared 0D Cs₄PbBr₆ was then separated by centrifugation for 15 min at 6000 rpm, followed by resuspension in hexane at 4 °C for further use. We determined the element molar ratios using inductively coupled plasma-mass spectrometry (ICP-MS) data. As reported in Figure 1, the transmission electron microscopy (TEM) image from freshly prepared 0D Cs₄PbBr₆ perovskite is highly monodisperse with size of 30 ± 3 nm and has no luminescence before immersing in water. The HRTEM image, as inserted in Figure 1, shows clear lattice fringes with interplanar spacing (d) of \sim 0.56 nm corresponding to the (110) crystal plane of Cs₄PbBr₆. The X-ray powder diffraction (XRD) data from 0D Cs₄PbBr₆, as reported in Figure 2A, show that it retains the rhombohedral phase, where main peaks are assigned to be (120), (113), (300), (020), (301), (223), (214), (314), (324), and (311) planes. ²⁰⁻⁴⁰ As shown in Figure 1 and Table 1, in the next step, nanowires, nanosheets, and nanocubes were obtained through an interfacial conversion from 0D Cs₄PbBr₆ nanocrystals by water induction.

For the development of 3D $CsPbBr_3$ nanocubes, we used 1 mM of Cs_4PbBr_6 solution in hexane. We also added 0.2 mL of water and kept it undisturbed for several hours at room

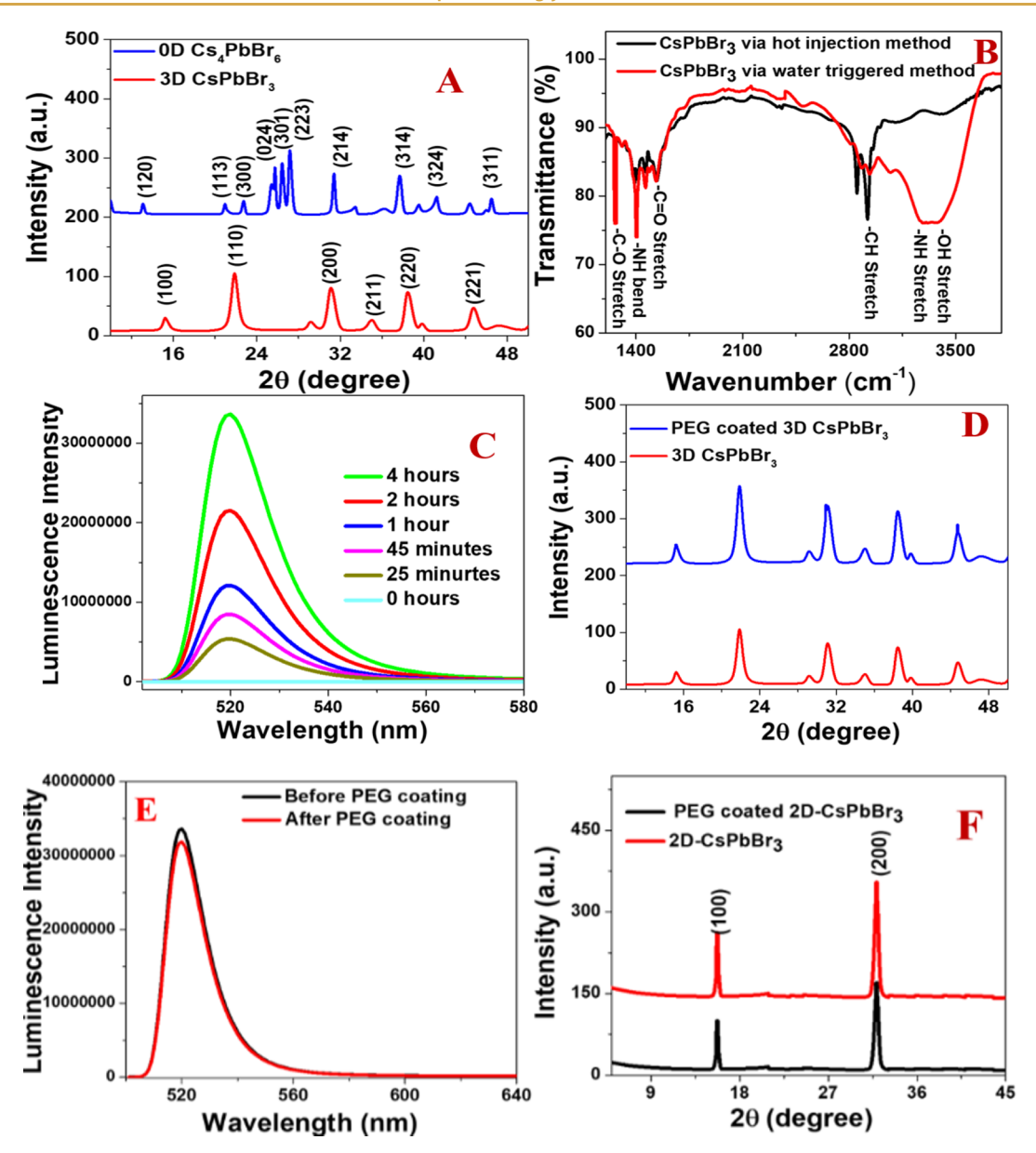


Figure 2. (A) X-ray diffraction patterns from 0D Cs₄PbBr₆ (JCPDS No. 73-2478) and 3D CsPbBr₃ nanocrystals (JCPDS No. 054-752). (B) FTIR spectra from 3D CsPbBr₃ made using the hot injection method and PEG coated 3D CsPbBr₃. (C) Change in fluorescence intensity after adding water to 0D Cs₄PbBr₆ solution in hexane during the formation of 3D nanocrystals. (D) X-ray diffraction patterns from 3D CsPbBr₃ nanocrystals and PEG coated 3D CsPbBr₃. (E) Luminescence spectra from 3D CsPbBr₃ nanocubes and PEG coated 3D CsPbBr₃ nanocubes. (F) X-ray diffraction patterns from nanoplatelets and PEG coated nanoplatelets (JCPDS No. 18-0364).

temperature. Upon contact with water, colorless Cs_4PbBr_6 solution rapidly became greenish, which indicates the formation of 3D $CsPbBr_3$ nanocubes. To understand the evolution of the process from zero dimensional Cs_4PbBr_6 nanocrystals to 3D $CsPbBr_3$ nanocubes, we monitored the time-dependent emission spectra during the synthesis process. As shown in Figure 2C, a green emission peak appears with luminescence maximum at 528 nm even within 25 min and continually increases as the reaction proceeds.

During this process, stripping of CsBr occurs because of the ionic nature of Cs₄PbBr₆ and the very high solubility of CsBr in water. The above process helps the decomposition of Cs₄PbBr₆ and the formation of the simple cubic structure of 3D CsPbBr₃. When the CsPbBr₃ nanocubes are formed, they diffused to the top, and as a result, we observed the greenish color at the water surface. It is now well-documented that the

capping oleic acid (OA) and olamine (OAm) ligands are mostly coordinating at Pb sites. 33-43

In the presence of minor amounts of water, H_2O molecules can partly ionize into H_3O^+ and OH^- with the help of OA and OAm. $^{30-44}$ In the next step, OH^- can partially replace OA or OAm on the surface. In this condition, the structure became loose, which allowed it to form decoupled $[PbBr_6]^{4-}$ octahedrons. $^{28-36}$ These octahedral monomers help to form bigger hexagonal particles, which allows them to develop 3D CsPbBr $_3$ nanocubes, and they are protected by the hydroxy (OH) group. $^{33-43}$

After the full transformation, CsPbBr₃ nanocrystals were isolated by centrifuging at 8000 rpm for 5 min to obtain high-quality nanocubes. TEM image from freshly prepared 3D CsPbBr₃, as reported in Figure 1, and dynamic light scattering (DLS) data, as reported in Table 2, show that the perovskites

Table 1. Variation of the % of 0D Cs₄PbBr₆, 1D, 2D, and 3D CsPbBr₃ NCs in the Presence of Different Amount of Water^a

amount of water (mL)	% of 0D Cs ₄ PbBR ₆	% of 3D CsPbBr ₃ nanocubes	% of 2D CsPbBr ₃ small nanosheets	% of 2D CsPbBr ₃ nanoplatelets	% of 2D CsPbBr ₃ big nanosheets	% of 1D CsPbBr ₃ nanowires
0	100	0	0	0	0	0
0.05	60	40	0	0	0	0
0.1	20	80	0	0	0	0
0.2	0	100	0	0	0	0
0.5	0	80	20	0	0	0
1.0	0	50	50	0	0	0
3.0	0	0	35	65	0	0
5.0	0	0	0	100	0	0
7.0	0	0	0	40	60	0
10.0	0	0	0	5	70	25
13.0	0	0	0	0	30	70
15.0	0	0	0	0	0	100

^aThe percentages of different shapes were calculated from the TEM image. For this purpose, we used 10 TEM pictures and averaged them.

Table 2. Relationship between the Amount of Water and the Morphology of 1D, 2D, and 3D CsPbBr₃ NCs^a

amount of water	morphology	size (nm, measured by TEM)	size (nm, measured by DLS)	emission maxima (nm)	IP PLQY (%)	2P absorption cross section
0.2	nanocubes	$L=25\pm 5$	28 ± 6	528	~68	8.1×10^{4}
5.0	nanoplatelet	$L = 20 \pm 4$	20 ± 5	484	~86	4.8×10^{5}
		$T = 4 \pm 1$				
15.0	nanowire	$L = 200 \pm 50$	220 ± 70	534	~76	2.3×10^{5}
		$T = 10 \pm 2$				

[&]quot;Size distribution for 1D, 2D, and 3D CsPbBr₃ NCs measured by TEM/SEM and DLS. Single-photon and two-photon optical properties for 1D, 2D, and 3D CsPbBr₃ NCs.

are highly monodispersed with size of 25 ± 5 nm. The HRTEM image as inserted in Figure 1 shows clear lattice fringes with interplanar spacing (d) of \sim 0.55 nm corresponding to the (110) crystal plane of the CsPbBr₃ cubic phase. As shown in Figure 2A, 3D CsPbBr₃ is retained the cubic phase, where main peaks are assigned to be the (100), (110), (111), (200), (211), and (220) planes of the cubic lattice. The photoluminescent quantum yield for 3D CsPbBr₃ was measured to be \sim 68%. Figure 3E shows that the stability in water for 3D CsPbBr₃ developed using the water-triggered process is much better than that of 3D CsPbBr₃ developed using the hot injection method, which can be attributed to the protection by the surface -OH groups.

To understand how the water amount variation can change the morphology of the product, we performed the same experiment by varying the water amount from 0.05 to 0.2 mL and keeping the Cs₄PbBr₆ concentration the same. As reported in Table 1, when we used 0.05 mL of water, we obtained 60% 0D Cs₄PbBr₆ and 40% 3D CsPbBr₃. As we increased the amount of water from 0.05 to 0.1 mL, we obtained 20% 0D Cs₄PbBr₆ and 80% 3D CsPbBr₃. At the end, when we used 0.2 mL water, we obtained 100% 3D CsPbBr₃.

In the next step for the development of biocompatible 3D CsPbBr₃ nanocrystals, we redispersed the nanocrystal in water with PEG under stirring for 40 min. Finally, the suspension was sonicated for a few minutes, and PEG coated nanocrystals were collected through filtration. As reported in Figure S1A, B, the TEM image from freshly prepared PEG coated 3D CsPbBr₃ shows that the size variation is within 35 ± 5 nm. The increase in size from 25 ± 5 to 35 ± 5 nm is mainly due to the coating of PEG. FTIR spectra as reported in Figure 2B shows –OH vibrational peaks from PEG coated 3D CsPbBr₃, which is mainly due to hydroxy coating originated during water triggered synthesis. We also observed peaks for the C–O

stretch, -NH stretch, and -NH bend, which are due to the propionic acid-PEG-NH $_2$ coating. Other observed vibrational peaks are mainly due to OA and OAm. The XRD data, reported in Figure 2D, show that PEG coated 3D CsPbBr $_3$ does retain the cubic phase after it was encapsulated with polymers.

Amine–PEG–propionic acid (Mn, 1100) coated CsPbBr₃ nanocrystals were highly dispersed in water for several weeks. We did not observe any aggregation even after 21 days. To understand how the variation of PEG concentration affects the water dispersity and single- and two-photon luminescence behavior of CsPbBr₃ nanocrystals, we performed the PEG coating experiment with the change in concentration of PEG from 0.5 to 10 mg/mL. From the experimental observation, we found that the water dispersity increases as we increase concentration of PEG from 0.5 to 5 mg/mL, and after that, it remains constant with the increase in PEG concentration.

On the other hand, single- and two-photon luminescence behavior remains the same as we increase the concentration of PEG from 0.5 to 3 mg/mL. After that, the PLQY decreases with the increase in concentration of PEG. As a result, for our experiment, we used 3 mg/mL PEG.

The photograph reported as Figure S1C, D and the luminescence spectra as reported in Figure 2E show that the luminescence color and spectra remain the same after polymer coating. The photoluminescence quantum yield for 3D CsPbBr₃ nanocubes is measured using eq 1, 15-30

$$PLQY = N_{emit}/N_{absorb}$$
 (1)

where $N_{\rm emit}$ and $N_{\rm absorb}$ are numbers of emitted and absorbed photons, respectively, for 3D CsPbBr₃. From the experimental measurement, we estimated that the photoluminescent quantum yield for PEG coated 3D CsPbBr₃ is ~66%.

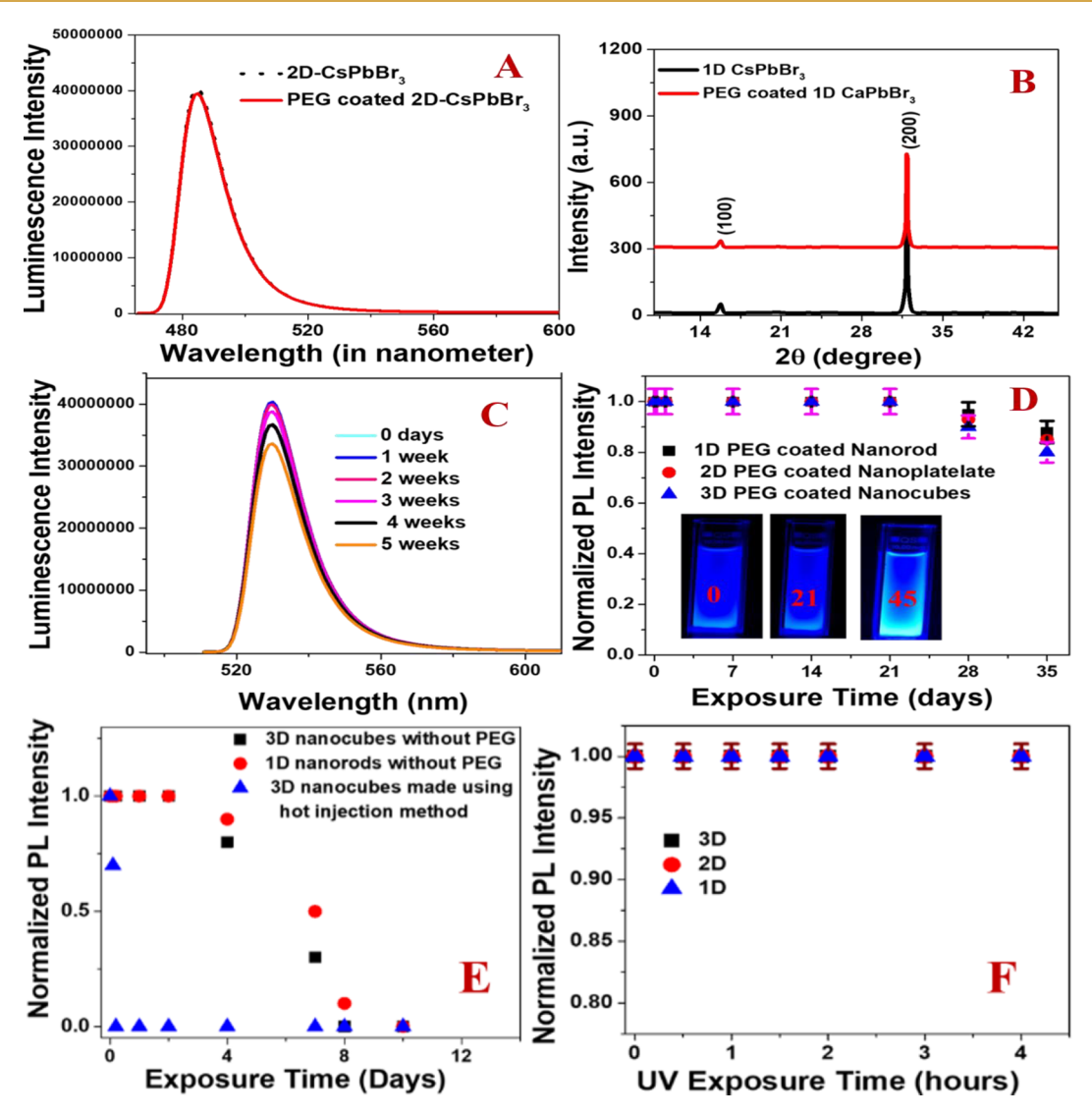


Figure 3. (A) Luminescence spectra from 2D nanoplatelets and PEG coated 2D nanoplatelets. (B) X-ray diffraction patterns from 1D nanowires and PEG coated 1D nanowires (JCPDS No. 01-072-7929). (C) Change of luminescence intensity with time when PEG coated 1D nanowires were placed under water for several weeks. (D) Change of normalized PL intensity (PL intensity at certain time/PL intensity initially) with time for PEG coated 1D, 2D, and 3D CsPbBr₃ nanocrystals when they are kept under water. Inserted picture shows how luminescence color under UV light changes for PEG coated 2D nanoplatelets in water at 0, 21, and 45 days. (E) Change of normalized PL intensity with time for water driven synthesis of 1D and 3D CsPbBr₃ nanocrystals when they are kept under water. The same graph also compares the change of normalized PL intensity with time for 3D nanocubes derived from the hot injection method. (F) How PL intensity for PEG coated 1D, 2D, and 3D CsPbBr₃ nanocrystals varies during exposure to UV light. We used 360 nm UV-light with 30 mW/cm² power.

Figure 3C and D shows that the stability in water for PEG coated 3D CsPbBr₃ is excellent, and our data indicate that more than 86% IP luminescence intensity remains after 35 days under water. On the other hand, as reported in Figure 3E, luminescence intensity became zero after 8 days under water for 3D CsPbBr₃ without PEG and was developed using water triggered method. All the above experimental data clearly show that for long-term stability, the PEG coating is very important.

The linear absorption cross-section ($\sigma_{\rm lin}$) and molar extinction coefficients (ε) for the PEG coated 3D CsPbBr₃ nanocubes were determined using inductively coupled plasma mass spectrometry (ICP-MS) combined with UV-vis, as we and others have reported before. ^{9,10,28,47} From the elemental analysis data, we obtained $\sigma_{\rm lin} = 1.6 \times 10^{-14}$ cm² PEG coated 3D CsPbBr₃ nanocubes at 400 nm. We also confirmed the values using one-photon induced ground state bleaching (GSB) data derived from femtosecond-transient absorption

spectroscopy. ^{48–52} From the transient absorption spectroscopy data, we obtained $\sigma_{\rm lin} = 1.2 \times 10^{-14}~\rm cm^2$ at 400 nm. From the $\sigma_{\rm lin}$ value, we determined the ε for PEG coated 3D CsPbBr₃ nanocubes, which was $\sim 3.1 \times 10^6~\rm L~cm^{-1}~mol^{-1}$ at 400 nm. Experimental data match quite well with the reported values. ^{50–52}

It is now well-documented that ^{28–40} the photostability of CsPbX₃ perovskites is a very important issue for their practical applications in optical devices. To determine the photostability of the PEG coated CsPbX₃ perovskites, we exposed perovskites with 360 nm UV-light irradiation. For this purpose, we exposed 30 mW/cm² power UV light for several hours. We monitored how PL intensity changes during the exposure to UV light. Figure 3F shows very good photo stability for PEG coated 3D CsPbBr₃ nanocubes when they are placed under UV light for several hours.

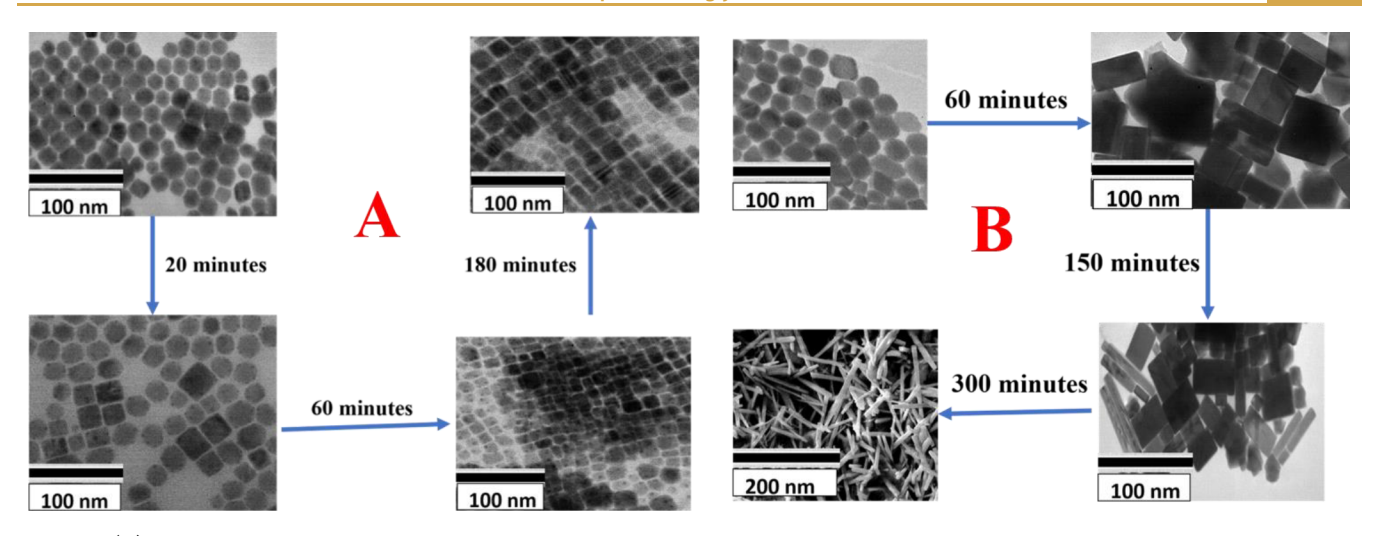


Figure 4. (A) Time dependent TEM image data show evolution of Cs₄PbBr₆ NCs to 2D CsPbBr₃ nanoplatelets through self-organization during water triggered synthesis. (B) Time-dependent TEM image data show evolution of Cs4PbBr₆ NCs to 1D CsPbBr₃ nanowires through self-organization during water triggered synthesis.

2.2. Water Triggered Synthesis of 2D CsPbBr₃ Nanoplatelets from 0D Cs₄PbBr₆ Nanocrystals Using 5 mL of Water

For the development of 2D CsPbBr₃ nanoplatelets, we used 1 mM of Cs₄PbBr₆ solution in hexane and added 5 mL of water. We kept the solution undisturbed for several hours at room temperature. It is very interesting to note that just by varying the amount of water, we can vary the dimension of CsPbBr₃ perovskite crystals. To understand the evolution process from 0D Cs₄PbBr₆ nanocrystals to 2D CsPbBr₃ nanoplatelets, we performed a time dependent TEM study, as reported in Figure 4A. TEM data show that within 20 min, nanocubes start forming, and as a result, we observed a mixture of 0D Cs₄PbBr₆ and 3D CsPbBr₃ nanocubes after 20 min of the water triggered synthesis process. After 80 min of the water triggered synthesis process, we observed the combination of 3D CsPbBr₃ nanocubes, 2D nanosheets, and 2D nanoplatelets. As shown in Figure 4A, after 260 min of the water triggered synthesis process, we observed mainly 2D nanoplatelets. As we have discussed before, during the water triggered synthesis process, dropping of CsBr into water happens through the interface. 30-40 It is possible that when we use 0.2 mL of water, the amount of water is enough to form only cubic crystals. In the presence of more water (5 mL in this case), more and more capping ligands are partially detached from the surface, and a higher amount of [PbBr₆]⁴⁻ octahedrons are formed in the system. As a result, the stability of the initial hexagons became lower. In this condition, formation of 2D CsPbBr3 nanoplatelets occurs through a self-organization process, as shown in Figure 4. The XRD spectra reported in Figure 2F show only two peaks which correspond to (100) and (200). XRD results and TEM images reported in Figures 1 and 4 evidently reveal that the final product is 2D CsPbBr3 nanoplatelets. Reported TEM data and DLS data in Table 2 indicate that the size of nanoplatelets is \sim 20 \pm 4 nm and the thickness is \sim 4 nm. The HRTEM image, as inserted in Figure 1, shows clear lattice fringes with interplanar spacing (d) of \sim 0.29 nm corresponding to the (200) crystal plane of CsPbBr₃.

To understand how varying the water amount can change the morphology of the product, we performed the same experiment by varying the water amount from 0.5 to 5 mL and keeping Cs_4PbBr_6 concentration the same. As reported in

Table 1, when we used 0.5 mL of water, we obtained 80% 3D CsPbBr₃ nanocubes and 20% 2D small nanosheets. As we increased the amount of water from 0.5 to 3 mL, we obtained 35% 2D small nanosheets and 65% 2D CsPbBr₃ nanoplatelets. At the end, when we used 5 mL of water, we obtained 100% 2D CsPbBr₃ nanoplatelets.

The photoluminescent quantum yield for 2D CsPbBr₃ nanoplatelets was measured to be ~86% using eq 1, which is mainly due to the quantum confining effect. S-20 Because the thickness of 2D CsPbBr₃ nanoplatelets (4 nm) is much less than the Bohr diameters for CsPbBr₃ (7 nm), 1-10 one can expect excellent quantum confinement. In the next step, we developed PEG coated nanocrystals using the method we have discussed before. The XRD data, as reported in Figure 2F, show that PEG coated 2D CsPbBr₃ nanoplatelets does retain the same phase with 2D CsPbBr3 nanoplatelets before encapsulation. The photoluminescent quantum yield for PEG coated 2D CsPbBr₃ nanoplatelets was measured to be ~84%. Figure 3D show that the stability in water for PEG coated 2D CsPbBr₃ nanoplatelets is excellent and experimental data show that more than 80% IP luminescence intensity remain after 35 days under water.

From the elemental analysis data, we obtained $\sigma_{\rm lin}=4.2\times 10^{-14}~{\rm cm}^2$ for PEG coated 2D CsPbBr₃ nanoplatelets at 400 nm. From $\sigma_{\rm lin}$ value we determined the ε for 2D CsPbBr₃ nanoplatelets, which was $\sim 9.2\times 10^6~{\rm L~cm}^{-1}~{\rm mol}^{-1}$ at 400 nm. Experimental data match quite well with the reported values. $^{50-52}$

2.3. Water Triggered Synthesis of 1D CsPbBr₃ Nanowires from 0D Cs₄PbBr₆ Nanocrystals Using 15 mL of Water

For the development of 1D CsPbBr $_3$ nanowires, we used 6 mM of Cs $_4$ PbBr $_6$ solution in cyclohexane and we added 15 mL of water. We kept it undisturbed for several hours at room temperature. To understand the possible mechanism, we performed time dependent TEM study as reported in Figure 4B. TEM data show that within 60 min of the water triggered synthesis process, big size 2D-CsPbBr $_3$ large nanosheets are formed. After 210 min of the water triggered synthesis process, we observed the combination if 2D nanosheets and 1D nanowires.

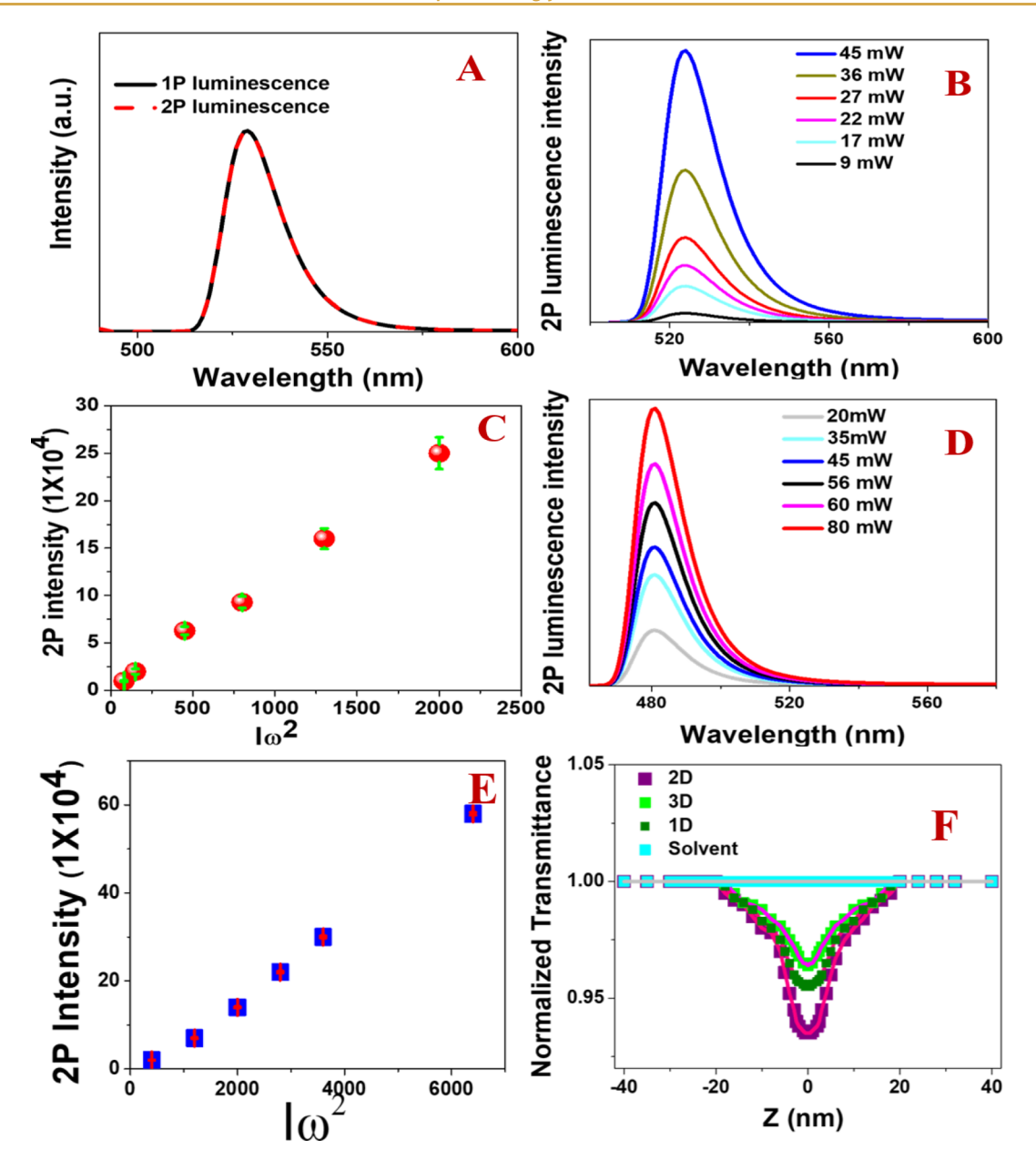


Figure 5. (A) Normalized 1P and 2P PL spectra from 1D CsPbBr₃ nanowires. (B) 2PL spectra from 3D CsPbBr₃ nanocubes at 800 nm excitation for several excitation laser power levels. (C) Figure shows how 2PL intensity from 3D CsPbBr₃ nanocubes varies with $I\omega^2$ for 800 nm excitation light. (D) 2PL spectra from 2D CsPbBr₃ nanoplatelets at 800 nm excitation for several excitation laser power levels. (E) Figure shows how 2PL intensity from 2D CsPbBr₃ nanoplatelets varies with $I\omega^2$ for 800 nm excitation light. (F) Open-aperture Z-scan curves for 2D CsPbBr₃ nanoplatelets, 3D CsPbBr₃ nanocubes, 1D CsPbBr₃ nanowires and solvent.

As shown in Figure 4B, after 510 min of the water triggered synthesis process, we observed 100% of 1D nanowires. As we have discussed before, water, as a polar solvent, can help to activate the nanocrystal surface by decreasing the surface density of the capping ligand. The above process also increases $[PbBr_6]^{4-}$ octahedron concentration by redissolving some of the already formed nanocubes, which will yield a higher growth rate^{1a-i}. Because both H_3O^+ and OH^- can act as surface ligands with higher activity as compared to OA and OAm, in the presence of water, it changes the perovskite orientation growth to form nanowires, which could lower the surface energy. The XRD spectra reported in Figure 3B shows only two peaks which corresponding to (100) and (200). XRD result and TEM image reported in Figure 1 and Figure 5 evidently reveal that the final product is 1D CsPbBr₃

nanowires. Reported TEM data in Figures 1 and 5 and DLS data as reported in Table 2, indicate that the length of nanowires is $\sim 200 \pm 50$ nm and diameter is ~ 10 nm. The HRTEM image, as inserted in Figure 1, shows clear lattice fringes with interplanar spacing (d) ~ 0.55 nm corresponding to the (100) crystal plane of CsPbBr₃.

To understand how the water amount variation can change the morphology of the product, we performed the same experiment by varying the water amount from 7 to 15 mL and keeping Cs₄PbBr₆ concentration the same. As reported in Table 1, when we used 7 mL water, we obtained 40% 2D CsPbBr₃ nanoplatelets and 60% 2D CsPbBr₃ big nanosheets. As we increased the amount of water from 7 to 13 mL, we obtained 30% 2D CsPbBr₃ big nanosheets and 70% 1D CsPbBr₃ nanowires. At the end when we used 15 mL water, we

obtained 100%1D CsPbBr₃ nanowires. The photoluminescent quantum yield for 1D CsPbBr₃ nanowires was measured to be ~76% using eq 1. The obtained high PLQY is mainly due to the quantum confine effect to some extent. Because the thickness of 1D CsPbBr₃ nanowires (8 nm), which is slightly higher than Bohr diameters for CsPbBr₃ (7 nm), one can expect quantum confinement to some extent. In the next step, we developed PEG coated nanocrystals using the method we have discussed before.

The XRD data, reported in Figure 3B, show that PEG coated 1D $CsPbBr_3$ nanowires do retain the same phase with 1D $CsPbBr_3$ nanowires before encapsulation. The photoluminescent quantum yield for PEG coated 2D $CsPbBr_3$ nanoplatelets was measured to be \sim 74%. Figure 3D shows that the stability in water for PEG coated 1D $CsPbBr_3$ nanowires is excellent, and experimental data show that more than 85% IP luminescence intensity remains after 35 days under water.

From the elemental analysis data, we obtained $\sigma_{\rm lin}=3.4\times 10^{-14}~{\rm cm}^2$ for PEG coated 1D CsPbBr $_3$ nanowires at 400 nm. From the $\sigma_{\rm lin}$ value, we determined ε for 1D CsPbBr $_3$ nanowires, which was $\sim 7.3\times 10^6~{\rm L~cm}^{-1}~{\rm mol}^{-1}$ at 400 nm. Experimental data match quite well with the reported values. $^{50-52}$

Figure 3F shows very good photostability for PEG coated 1D CsPbBr₃ nanorods when they are place under UV light for several hours. Strong PLQY and excellent photostability and water resistance make PEG coated 1D, 2D, and 3D-CsPbBr₃ nanocrystals very good candidates for bioimaging applications.

2.4. Two-Photon Absorption Properties for 1D, 2D, and 3D CsPbBr₃ Nanocrystals

We used TPL spectroscopy and Z-scan technique for the determination of the two-photon absorption properties for PEG coated 1D, 2D, and 3D CsPbBr₃ nanocrystals. $^{45-54}$ Experimental details have been reported before and are discussed in the Supporting Information. $^{47,55,58-60,68-71}$ In brief, for the measurement, we used an 80 MHz Ti-sapphire laser as an excitation source with 100 fs pulse width. $^{47,55,58-60}$ We used an optical parametric amplifier to generate 800 nm excitation wavelength. 3,47,55,58,60 The laser beam was focused down to a radius of ~30 μ m on the sample.

To determine the photostability of the PEG coated CsPbX₃ perovskites during 2P absorption and Z-scan experiments, we determined how PL intensity changes during the exposure to 800 nm NIR light. For this purpose, we used 100 mW 800 nm light. As shown in Figure S2A in the Supporting Information, PL intensity for PEG coated 1D CsPbBr₃ nanocrystals remains about same during the exposure to 800 nm NIR light for 15 min. Because in the 2P and Z-scan experiments 800 nm light exposure time is less than 10 min, the photostability for CsPbBr₃ nanocrystals will remain the same. We also performed an XRD experiment before and after the 2P experiment. XRD data reported in Figure S2B indicate that CsPbBr₃ nanocrystals are retained in the same phase, which indicates no optical damage within our experimental time range.

Figure 5A shows the normalized 1P and 2P luminescence spectra from 1D CsPbBr₃ nanowires using 400 and 800 nm excitation light, which indicates that one- and two-photon absorption are very identical. It may be because the nanocrystals excited by either 1P or 2P absorption will relax to the same lowest excited state. 45-54 To understand better, we also performed the excitation intensity dependent 2P

luminescence measurements. As shown in Figures 5B–E, the quadratic dependence of the luminescence intensity from 3D CsPbBr₃ nanocubes and 2D CsPbBr₃ nanoplatelets clearly confirms the 2P processes. The absolute two-photon absorption cross sections for PEG coated 1D, 2D, and 3D CsPbBr₃ nanocrystals were determined using fluorescein as a reference, whose 2PA is known in literature. Using the reference, 2PA cross-section for PEG coated 1D CsPbBr₃ nanowires was determined using eq 2.44–54

$$\sigma_{\text{nanowires}} = \sigma_{\text{FL}}(F_{\text{nanowires}}/F_{\text{FL}})(\Phi_{\text{FL}}/\Phi_{\text{nanowires}})$$

$$(C_{\text{FL}}/C_{\text{nanowires}}) \tag{2}$$

where F is the observed fluorescence intensity from fluorescein and PEG coated 1D CsPbBr₃ nanowires. Similarly, Φ is the quantum yield, and C is the concentration of fluorescein and PEG coated 1D CsPbBr₃ nanowires. For the TPL experiment, we used ~100 nM CsPbBr₃ nanocrystals. Using experimental data, we determined the two-photon absorption cross sections for 1D CsPbBr₃ nanowires to be 5.1 \times 10⁵ GM at 800 nm excitation. We also determined the 2P cross-section using the Z-scan technique, 45-54 as shown in Figure 5F. The transmission for open aperture Z-scan was measured using eq 3^{44-54} for PEG coated 1D, 2D, and 3D CsPbBr₃ nanocrystals,

$$T_{\text{open}}(Z) = 1 - 1/2\sqrt{2} \left[(\alpha_{\text{NL}} I_0 L_{\text{eff}}) \right] / \left[1 + (z/z_0)^2 \right]$$
 (3)

where $L_{\text{eff}} = (1 - e^{-\alpha} {}^{L})/\alpha_0$, and L is the sample thickness for PEG coated 1D, 2D, and 3D CsPbBr₃ nanocrystals. Similarly, I_0 is the on-axis peak intensity. z is the longitudinal displacement of the sample from the focus, and z_0 is the Rayleigh diffraction length. After subtraction of the solvent contribution to the measured two-photon signal, we determined the 2PA absorption coefficients for PEG coated 1D, 2D, and 3D CsPbBr₃ nanocrystals. Using Z-scan data, we determined 2PA coefficients of PEG coated 1D, 2D, and 3D nanocrystals, and these are $\sigma_2 \sim 2.3 \times 10^5$ GM for 1D nanowires, $\sigma_2 \sim 4.8 \times 10^5$ GM for 2D nanoplatelets, and $\sigma_2 \sim$ 8.1×10^4 GM for 3D nanocubes (1 GM = 1×10^{-50} cm⁴·s· photon⁻¹), which are several orders of magnitude higher than that of organic chromophores (>100 GM). Reported 2P crosssections for 2D and 3D nanocrystals match very well with the reported data.44-54

Because the volumes of 1D, 2D, and 3D nanocrystals are different, we calculated volume-normalized 2PA cross sections (in GM nm⁻³) for 1D, 2D, and 3D nanocrystals, and these are $\sigma_2 \sim 28.5 \text{ (GM nm}^{-3}) \text{ for 1D nanowires, } \sigma_2 \sim 430 \text{ (GM nm}^{-3})$ for 2D nanoplatelets, and $\sigma_2 \sim 9.2$ (GM nm⁻³) GM for 3D nanocubes. Our observed highest VN 2PA cross-section for 2D nanoplatelets can be due the higher transition dipole moment attributed to stronger confinement effect than that of 3D nanocubes and 1D nanowires. 50,53,54 To understand whether the PEG coating enhances the 2PA cross-section for 1D, 2D, and 3D CsPbBr3 nanocrystals, we also measured the 2PA cross-section for 1D, 2D, and 3D CsPbBr3 nanocrystals with PEG. Using Z-scan data, we determined 2PA coefficients of 1D, 2D, and 3D nanocrystals, and these are $\sigma_2 \sim 2.1 \times 10^5$ GM for 1D nanowires, $\sigma_2 \sim 4.9 \times 10^5$ GM for 2D nanoplatelets, and $\sigma_2 \sim 8.5 \times 10^4$ GM for 3D nanocubes, which are very similar to the 2PA properties for PEG coated 1D, 2D, and 3D CsPbBr₃ nanocrystals.

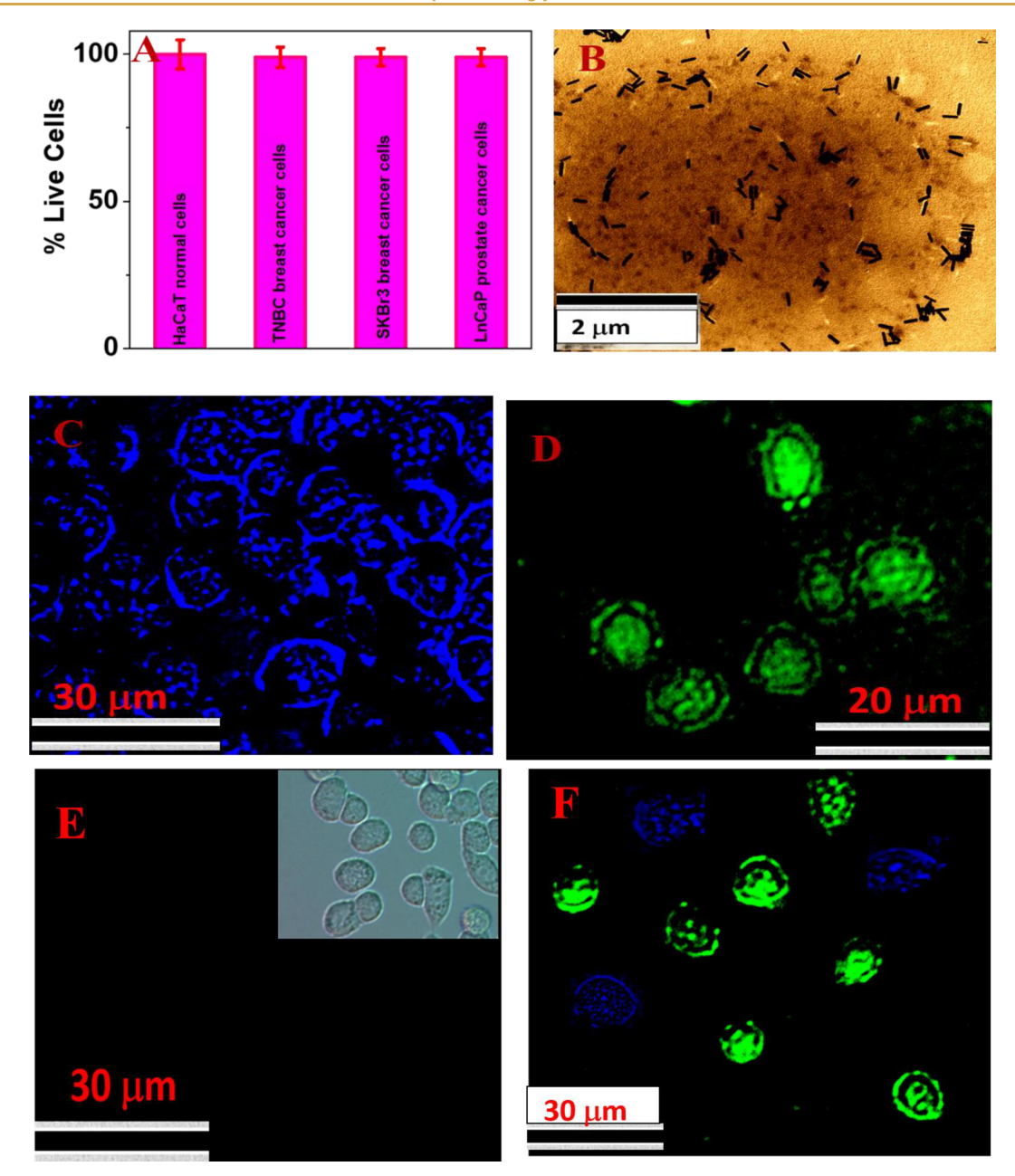


Figure 6. (A) Plot showing biocompatibility for 2D CsPbBr $_3$ nanoplatelets for different cancer cells and normal skin cells. (B) TEM image of anti-HER-2 antibody conjugated 1D CsPbBr $_3$ nanowire attached HER-2(+) SK-BR-3 breast cancer cells. (C) Two-photon luminescence image from PR(-) ER(-) HER-2(-) MDA-MB-231 breast cancer cells which are attached to anti-AXL antibody conjugated 2D CsPbBr $_3$ nanoplatelets. (D) Two-photon luminescence image from HER-2(+) SK-BR-3 breast cancer cells which are attached to anti-HER-2 antibody conjugated 1D CsPbBr $_3$ nanowires. ((E) Two-photon luminescence image from HER-2(-) MDA-MB-231 TNBC cells in the presence of anti-HER-2 antibody conjugated 1D CsPbBr $_3$ nanowires. Inserted bright field image shows the presence of HER-2(-) MDA-MB-231 TNBC cells. No luminescence was observed, which indicates that anti-HER-2 antibody conjugated 1D CsPbBr $_3$ nanowires do not bind with HER-2(-) MDA-MB-231 TNBC cells. (F) Two-photon luminescence image from a mixture of PR(-) ER(-) HER-2(-) MDA-MB-231 breast cancer and HER-2(+) SK-BR-3 breast cancer cells. For multicolor imaging, we used anti-AXL antibody conjugated 2D CsPbBr $_3$ nanoplatelets and anti-HER-2 antibody conjugated 1D CsPbBr $_3$ nanowires together.

2.5. Two-Photon Imaging of Cancer Cells Using 1D, 2D, and 3D CsPbBr₃ Nanocrystals

Inspired by the excellent two-photon absorption coefficients, very good water resistance capability, and good photostability, we attempted to explore the use of anti-AXL antibody attached CsPbBr₃ nanoplatelet and anti-HER-2 antibody attached nanowire probes for tracking TNBC and HER-2(+) SK-BR-3 cells. Initially, we determined the biocompatibility for nanocrystals. For this purpose, we incubated PEG coated

nanocrystals with 2.6×10^5 cells per mL normal HaCaT skin cells, HER-2(+) SK-BR-3 cells, MDA-MB-231 TNBC cells, and LNCaP human prostate cancer cells separately for 24 h. After that, the numbers of live cells were measured using an MTT test. $^{55,58-60,65,66}$ As reported in Figure 6A, PEG coated 2D nanoplatelets show excellent biocompatibility. We have also performed a concentration dependent biocompatibility experiment for PEG coated 2D nanoplatelets using normal HaCaT skin cells, HER-2(+) SK-BR-3 breast cells, MDA-MB-

231 TNBC cells, and LNCaP human prostate cancer cells separately. As reported in Figures S3A–D, our experimental data show that PEG coated 2D nanoplatelets show excellent biocompatibility even at the concentration of 50 μ g/mL. The observed very good biocompatibility is mainly due to the presence of the PEG coating, which helps CsPbX₃ perovskites not to decompose when exposed to water.

After that, the antibody was attached to the PEG coated 2D nanoplatelets and 1D nanowires via noncovalent interaction through PEG. Next, different concentrations of antibodyconjugated nanocrystals were mixed with cancer cells for 30 min. In the next step, unbound antibody-conjugated nanocrystals were separated using centrifugation. For the twophoton cancer imaging experiment, we used a Nikon multiphoton microscope (FV1000MPE), as we reported before. 55,58-60,65,66 Figure 6B shows that anti-HER-2 antibody conjugated nanocrystals are attached to the surface of HER-2(+) SK-BR-3 breast cancer cells. Figure 6C shows that anti-AXL antibody conjugated 2D nanoplatelets can be used for blue color two-photon imaging of TNBC cells. Similarly, Figure 6D shows that anti-HER-2 antibody conjugated 1D nanowires can be used for green color two-photon imaging of HER-2 (+) SK-BR-3 cells. The bright field images are reported in Figures S4A-C in the Supporting Information.

To find out the selectivity, we performed the experiment for HER-2(-) TNBC cells using anti-HER-2 antibody conjugated 1D nanowires. As reported in Figure 6E, we did not observe any luminescence image because anti-HER-2 antibody conjugated 1D CsPbBr3 nanowires do not bind with HER-2(-) MDA-MB-231 TNBC cells. The above data indicate that antibody attached 1D, 2D, and 3D CsPbBr3 nanocrystals are highly selective for targeted cancer cells. Next, we determined whether a mixture of anti-HER-2 antibody attached 1D nanowires and anti-AXL antibody conjugated 2D nanoplatelets can be used for the simultaneous identification of MDA-MB-231 TNBC cells and HER-2(+) breast cancer cells together. Figure 6F shows a multicolor blue/green two-photon luminescence image which shows that HER-2(+) SK-BR-3 cells and MDA-MB-231 TNBC cells can be simultaneously imaged using 2D nanoplatelets and 1D nanowires.

3. CONCLUSIONS

In conclusion, our findings reveal that water resistant, biocompatible, and photostable 1D CsPbBr₃ nanowires, 2D CsPbBr₃ nanoplatelets, and 3D CsPbBr₃ nanocubes can be designed through an interfacial conversion from 0D Cs₄PbBr₆ nanocrystals via a water triggered strategy using water and PEG. Reported data show that just by varying the amount of water one can control the dimension of CsPbBr3 perovskite crystals. Time dependent TEM and emission data show the possible pathway for the formation of 1D CsPbBr₃ nanowires, 2D CsPbBr₃ nanoplatelets, and 3D CsPbBr₃ nanocubes from 0D Cs₄PbBr₆ nanocrystals. Our experimental results find that these nanocrystals exhibit excellent IP luminescence PLQY and 2PL absorption coefficients. Reported data also show that more than 86% of IP luminescence intensity from PEG coated nanocrystals remained after 35 days under water. Experimental results show that selective and simultaneous two-photon imaging of TNBC cells and HER-2 (+) SKBR3 breast cancer cells in a near-IR biological window can be performed using specific antibody attached 1D and 2D perovskites.

As our reported data show, 1D CsPbBr₃ nanowires and 2D CsPbBr₃ nanoplatelets exhibit very high PLQY and good

photostability in water, which are much superior to that of commonly used organic probes; after proper engineering design, they will be better probes for bioimaging application. In addition, lead halide perovskite nanocrystals exhibit high absorption coefficients for two-, three- and five-photon processes, which is rare for commonly used organic probes that are used as fluorescence labels. These excellent properties provide advantages for all-inorganic cesium lead halide perovskite-based nanocrystals to be useful in the field of bioimaging. However, there are many issues that need to be addressed before 1D CsPbBr₃ nanowires and 2D CsPbBr₃ nanoplatelets can be used for real life applications, and these are stability in physiological conditions; possible toxicity due to degradation; interaction with DNA, RNA, and other biomolecules during circulation; epigenetic interaction, etc.

ASSOCIATED CONTENT

51 Supporting Information

The Supporting Information is available free of charge at https://pubs.acs.org/doi/10.1021/jacsau.0c00038.

Detailed synthesis, characterization of antibody attached nanowires, and other experiments (PDF)

AUTHOR INFORMATION

Corresponding Author

Paresh Chandra Ray — Department of Chemistry and Biochemistry, Jackson State University, Jackson, Mississippi 39217, United States; orcid.org/0000-0001-5398-9930; Email: paresh.c.ray@jsums.edu; Fax: +16019793674

Authors

Avijit Pramanik — Department of Chemistry and Biochemistry, Jackson State University, Jackson, Mississippi 39217, United States; orcid.org/0000-0002-4623-2099

Shamily Patibandla – Department of Chemistry and Biochemistry, Jackson State University, Jackson, Mississippi 39217, United States

Ye Gao – Department of Chemistry and Biochemistry, Jackson State University, Jackson, Mississippi 39217, United States

Kaelin Gates — Department of Chemistry and Biochemistry, Jackson State University, Jackson, Mississippi 39217, United States

Complete contact information is available at: https://pubs.acs.org/10.1021/jacsau.0c00038

Notes

The authors declare no competing financial interest.

ACKNOWLEDGMENTS

Dr. Ray is thankful for the generous funding from NSF-PREM Grant DMR-1826886 and NSF CREST Grant 1547754.

■ REFERENCES

- (1) Utzat, H.; Sun, W.; Kaplan, A. E. K.; Krieg, F.; Ginterseder, M.; Spokoyny, B.; Klein, N. D.; Shulenberger, K. E.; Perkinson, C. F.; Kovalenko, M. V.; Bawendi, M. G. Coherent Single-Photon Emission from Colloidal Lead Halide Perovskite Quantum Dots. *Science* **2019**, 363 (6431), 1068–1072.
- (2) Nayak, P. K.; Mahesh, S.; Snaith, H. J.; Cahen, D. Photovoltaic Solar Cell Technologies: Analysing the State of the Art. *Nat. Rev. Mater.* **2019**, *4*, 269–285.

- (3) Park, J.-M.; Park, J.; Kim, Y.-H.; Zhou, H.; Lee, Y.; Jo, S. H.; Ma, J.; Lee, T.-W.; Sun, J.-Y. Aromatic nonpolar organogels for efficient and stable perovskite green emitters. *Nat. Commun.* **2020**, *11* (1) DOI: 10.1038/s41467-020-18383-y.
- (4) Lin, K.; Xing, J.; Quan, L. N.; de Arquer, F. P. G.; Gong, X.; Lu, J.; Xie, L.; Zhao, W.; Zhang, D.; Yan, C.; Li, W.; Liu, X.; Lu, Y.; Kirman, J.; Sargent, E. H.; Xiong, Q.; Wei, Z. Perovskite Light-Emitting Diodes with External Quantum Efficiency Exceeding 20 per Cent. *Nature* 2018, 562, 245–248.
- (5) Quan, L. N.; Rand, B. P.; Friend, R. H.; Mhaisalkar, S. G.; Lee, T.-W.; Sargent, E. H. Perovskites for Next-Generation Optical Sources. *Chem. Rev.* **2019**, *119*, 7444–7477.
- (6) Shamsi, J.; Urban, A. S.; Imran, M.; De Trizio, L.; Manna, L. Metal Halide Perovskite Nanocrystals: Synthesis, Post-Synthesis Modifications, and Their Optical Properties. *Chem. Rev.* **2019**, *119*, 3296–3348.
- (7) Rainò, G.; Becker, M. A.; Bodnarchuk, M. I.; Mahrt, R. F.; Kovalenko, M. V.; Stöferle, T. Superfluorescence from Lead Halide Perovskite Quantum Dot Superlattices. *Nature* **2018**, *563* (7733), 671–675.
- (8) Lv, W.; Li, L.; Xu, M.; Hong, I.; Tang, X.; Xu, L.; Wu, Y.; Zhu, R.; Chen, R.; Huang, W. Improving the Stability of Metal Halide Perovskite Quantum Dots by Encapsulation. *Adv. Mater.* **2019**, *31*, 1900682.
- (9) Xing, J.; Zhao, Y.; Askerka, M.; Quan, L. N.; Gong, X.; Zhao, W.; Zhao, J.; Tan, H.; Long, G.; Gao, L.; Yang, Z.; Voznyy, O.; Tang, J.; Lu, Z.-H.; Xiong, Q.; Sargent, E. H. Color-stable highly luminescent sky-blue perovskite light-emitting diodes. *Nat. Commun.* **2018**, *9*, 3541.
- (10) Akkerman, Q. A.; Raino, G.; Kovalenko, M. V.; Manna, L. Genesis, challenges and opportunities for colloidal lead halide perovskite nanocrystals. *Nat. Mater.* **2018**, *17*, 394–405.
- (11) Phung, N.; Félix, R.; Meggiolaro, D.; Al-Ashouri, A.; Sousa e Silva, G.; Hartmann, C.; Hidalgo, J.; Köbler, H.; Mosconi, E.; Lai, B.; Gunder, R.; Li, M.; Wang, Z.-K.; Wang, K.-l.; Nie, K.; Handick, E.; Wilks, R. G.; Marquez, J. A.; Rech, B.; Unold, T.; Correa-Baena, J.-P.; Albrecht, S.; De Angelis, F.; Bär, M.; Abate, A. The doping mechanism of halide perovskite unveiled by alkaline earth metals. *J. Am. Chem. Soc.* 2020, 142 (5), 2364–2374.
- (12) DuBose, J. T.; Kamat, P. V. TiO2-Assisted Halide Ion Segregation in Mixed Halide Perovskite Films. *J. Am. Chem. Soc.* **2020**, 142 (11), 5362–5370.
- (13) Wang, S.; Du, L.; Jin, Z.; Xin, Y.; Mattoussi, H. Enhanced Stabilization and Easy Phase Transfer of CsPbBr3 Perovskite Quantum Dots Promoted by High-Affinity Polyzwitterionic Ligands. *J. Am. Chem. Soc.* **2020**, *142* (29), 12669–12680.
- (14) Peng, L.; Dutta, A.; Xie, R.; Yang, W.; Pradhan, N. Dot-Wire-Platelet-Cube: Step Growth and Structural Transformations in CsPbBr3 Perovskite Nanocrystals. ACS Energy Letters 2018, 3, 2014—2020.
- (15) Cho, J.; Kamat, P. V. How Chloride Suppresses Photoinduced Phase Segregation in Mixed Halide Perovskites. *Chem. Mater.* **2020**, 32, 6206–6212.
- (16) Kobosko, S. M.; DuBose, J. T.; Kamat, P. V. Perovskite Photocatalysis. Methyl Viologen Induces Unusually Long-Lived Charge Carrier Separation in CsPbBr3 Nanocrystals. *ACS Energy Lett.* **2020**, *5*, 221–223.
- (17) Hudait, B.; Dutta, S. K.; Patra, A.; Nasipuri, D.; Pradhan, N. Facets Directed Connecting Perovskite Nanocrystals. *J. Am. Chem. Soc.* **2020**, *142* (15), 7207–7217.
- (18) Pan, J.; Shang, Y.; Yin, J.; De Bastiani, M.; Peng, W.; Dursun, I.; Sinatra, L.; El-Zohry, A. M.; Hedhili, M. N.; Emwas, A.-H.; Mohammed, O. F.; Ning, Z.; Bakr, O. M. Bidentate Ligand-Passivated CsPbI₃ Perovskite Nanocrystals for Stable Near-Unity Photoluminescence Quantum Yield and Efficient Red Light-Emitting Diodes. *J. Am. Chem. Soc.* **2018**, *140*, 562–565.
- (19) Gao, M.; Liu, H.; Yu, S.; Louisia, S.; Zhang, Y.; Nenon, D. P.; Alivisatos, P.; Yang, P. Scaling Laws of Exciton Recombination

- Kinetics in Low Dimensional Halide Perovskite Nanostructures. J. Am. Chem. Soc. 2020, 142 (19), 8871–8879.
- (20) Dahl, J. C.; Wang, X.; Huang, X.; Chan, E. M.; Alivisatos, P. A. Elucidating the Weakly Reversible Cs—Pb—Br Perovskite Nanocrystal Reaction Network with High-Throughput Maps and Transformations. *J. Am. Chem. Soc.* **2020**, *142* (27), 11915—11926.
- (21) Cheng, P.; Sun, L.; Feng, L.; Yang, S.; Yang, Y.; Zheng, D.; Zhao, Y.; Sang, Y.; Zhang, R.; Wei, D.; Deng, W.; Han, K. Colloidal Synthesis and Optical Properties of All-Inorganic Low-Dimensional Cesium Copper Halide Nanocrystals. *Angew. Chem.* **2019**, *131* (45), 16233–16237.
- (22) Li, H.; Liu, X.; Ying, O.; Wang, C.; Jia, W.; Xing, X.; Yin, L.; Lu, Z.; Zhang, K.; Pan, Y.; Shi, Z.; Huang, L.; Jia, D. Self-Assembly of Perovskite CsPbBr 3 Quantum Dots Driven by a Photo-Induced Alkynyl Homocoupling Reaction. *Angew. Chem.* **2020**, *132* (39), 17360–17366.
- (23) Zhang, Y.; Lu, D.; Gao, M.; Lai, M.; Lin, J.; Lei, T.; Lin, Z.; Quan, L. N.; Yang, P. Quantitative Imaging of Anion Exchange Kinetics in Halide Perovskites. *Proc. Natl. Acad. Sci. U. S. A.* **2019**, *116* (26), 12648–12653.
- (24) Tong, Y.; Fu, M.; Bladt, E.; Huang, H.; Richter, A. F.; Wang, K.; Müller-Buschbaum, P.; Bals, S.; Tamarat, P.; Lounis, B.; Feldmann, J.; Polavarapu, L. Chemical Cutting of Perovskite Nanowires into Single-Photon Emissive Low-Aspect-Ratio CsPbX₃ (X = Cl, Br, I) Nanorods. *Angew. Chem., Int. Ed.* **2018**, *57* (49), 16094–16098.
- (25) Krieg, F.; Ong, Q. K.; Burian, M.; Raino, G.; Naumenko, D.; Amenitsch, H.; Süess, A.; Grotevent, M. J.; Krumeich, F.; Bodnarchuk, M. I.; Shorubalko, I.; Stellacci, F.; Kovalenko, M. V. Stable Ultraconcentrated and Ultradilute Colloids of CsPbX3 (X = Cl, Br) Nanocrystals Using Natural Lecithin as a Capping Ligand. *J. Am. Chem. Soc.* **2019**, *141*, 19839–19849.
- (26) Zhang, Q.; Yin, Y. All-Inorganic Metal Halide Perovskite Nanocrystals: Opportunities and Challenges. *ACS Cent. Sci.* **2018**, *4*, 668–679.
- (27) Dong, Y.; Qiao, T.; Kim, D.; Parobek, D.; Rossi, D.; Son, D. H. Precise Control of Quantum Confinement in Cesium Lead Halide Perovskite Quantum Dots via Thermodynamic Equilibrium. *Nano Lett.* **2018**, *18*, 3716–3722.
- (28) Pramanik, A.; Gates, K.; Patibandla, S.; Davis, D.; Begum, S.; Iftekhar, R.; Alamgir, S.; Paige, S.; Porter, M. M.; Ray, P. C. Water-Soluble and Bright Luminescent Cesium—Lead—Bromide Perovskite Quantum Dot—Polymer Composites for Tumor-Derived Exosome Imaging. ACS Appl. Bio Mater. 2019, 2, 5872—5879.
- (29) Zhang, X.; Bai, X.; Wu, H.; Zhang, X.; Sun, C.; Zhang, Y.; Zhang, W.; Zheng, W.; Yu, W. W.; Rogach, A. L. Water-Assisted Size and Shape Control of CsPbBr₃ Perovskite Nanocrystals. *Angew. Chem., Int. Ed.* **2018**, *57*, 3337–3342.
- (30) Jana, A.; Kim, K. S. Water-Stable, Fluorescent Organic—Inorganic Hybrid and Fully Inorganic Perovskites. *ACS Energy Lett.* **2018**, 3, 2120–2126.
- (31) Wu, L.; Hu, H.; Xu, Y.; Jiang, S.; Chen, M.; Zhong, Q.; Yang, D.; Liu, Q.; Zhao, Y.; Sun, B.; Zhang, Q.; Yin, Y. From Nonluminescent Cs₄PbX₆ (X= Cl, Br, I) Nanocrystals to Highly Luminescent CsPbX₃ Nanocrystals: Water-Triggered Transformation Through a CsX-Stripping Mechanism. *Nano Lett.* **2017**, *17*, 5799–580.
- (32) Yang, D.; Li, P.; Zou, Y.; Cao, M.; Hu, H.; Zhong, Q.; Hu, J.; Sun, B.; Duhm, S.; Xu, Y.; Zhang, Q. Interfacial Synthesis of Monodisperse CsPbBr3 Nanorods with Tunable Aspect Ratio and Clean Surface for Efficient Light-Emitting Diode Applications. *Chem. Mater.* **2019**, *31*, 1575–1583.
- (33) Li, Y.; Huang, H.; Xiong, Y.; Richter, A. F.; Kershaw, S. V.; Feldmann, J.; Rogach, A. L. Using Polar Alcohols for the Direct Synthesis of Cesium Lead Halide Perovskite Nanorods with Anisotropic Emission. *ACS Nano* **2019**, *13*, 8237–8245.
- (34) Yang, W.; Gao, F.; Qiu, Y.; Liu, W.; Xu, H.; Yang, L.; Liu, Y. CsPbBr₃-Quantum-Dots/Polystyrene@Silica Hybrid Microsphere

- Structures with Significantly Improved Stability for White LEDs. *Adv. Opt. Mater.* **2019**, 1900546.
- (35) Liu, Y.; Li, F.; Liu, Q.; Xia, Z. Synergetic Effect of Postsynthetic Water Treatment on the Enhanced Photoluminescence and Stability of CsPbX3 (X = Cl, Br, I) Perovskite Nanocrystals. *Chem. Mater.* **2018**, *30*, 6922–6929.
- (36) Zhong, Q.; Cao, M.; Xu, Y.; Li, P.; Zhang, Y.; Hu, H.; Yang, D.; Xu, Y.; Wang, L.; Li, Y.; Zhang, X.; Zhang, Q. L-Type Ligand-Assisted Acid-Free Synthesis of CsPbBr3 Nanocrystals with Near-Unity Photoluminescence Quantum Yield and High Stability. *Nano Lett.* **2019**, *19*, 4151–4157.
- (37) Wu, H.; Wang, S.; Cao, F.; Zhou, L.; Wu, O.; Wang, H.; Li, X.; Yin, L.; Yang, X. Ultrastable Inorganic Perovskite Nanocrystals Coated with a Thick Long-Chain Polymer for Efficient White Light-Emitting Diodes. *Chem. Mater.* **2019**, *31*, 1936–1940.
- (38) Tong, J.; Wu, J.; Shen, W.; Zhang, Y.; Liu, Y.; Zhang, T.; Nie, S.; Deng, Z. Direct Hot-Injection Synthesis of Lead Halide Perovskite Nanocubes in Acrylic Monomers for Ultrastable and Bright Nanocrystal—Polymer Composite Films. ACS Appl. Mater. Interfaces 2019, 11, 9317—9325.
- (39) Palazon, F.; Urso, C.; De Trizio, L.; Akkerman, Q.; Marras, S.; Locardi, F.; Nelli, I.; Ferretti, M.; Prato, M.; Manna, L. Postsynthesis Transformation of Insulating Cs₄PbBr₆ Nanocrystals into Bright Perovskite CsPbBr₃ Through Physical and Chemical Extraction of CsBr. ACS Energy Lett. **2017**, *2*, 2445–2448.
- (40) Pan, J.; Shang, Y.; Yin, J.; De Bastiani, M.; Peng, W.; Dursun, I.; Sinatra, L.; El-Zohry, A. M.; Hedhili, M. N.; Emwas, A.-H.; Mohammed, O. F.; Ning, Z.; Bakr, O. M. Bidentate Ligand-Passivated CsPbI₃ Perovskite Nanocrystals for Stable Near-Unity Photoluminescence Quantum Yield and Efficient Red Light-Emitting Diodes. *J. Am. Chem. Soc.* **2018**, *140*, 562–565.
- (41) Li, Z.; Kong, L.; Huang, S.; Li, L. Highly Luminescent and Ultrastable CsPbBr₃ Perovskite Quantum Dots Incorporated into a Silica/Alumina Monolith. *Angew. Chem.* **2017**, *129*, 8246–8250.
- (42) Li, S.; Lei, D.; Ren, W.; Guo, X.; Wu, S.; Zhu, Y.; Rogach, A. L.; Chhowalla, M.; Jen, A. K.-Y. Water-resistant perovskite nanodots enable robust two-photon lasing in aqueous environment. *Nat. Commun.* **2020**, *11*, 1192.
- (43) Song, G.; Li, M.; Zhang, S.; Wang, N.; Gong, P.; Xia, Z.; Lin, Z. Enhancing Photoluminescence Quantum Yield in 0D Metal Halides by Introducing Water Molecules. *Adv. Funct. Mater.* **2020**, *30* (32), 2002468.
- (44) Wei, Z.; Guo, D.; Thieme, J.; Katan, C.; Caselli, V. M.; Even, J.; Savenije, T. J. The importance of relativistic effects on two-photon absorption spectra in metal halide perovskites. *Nat. Commun.* **2019**, *10*, 5342.
- (45) Xu, J.; Li, X.; Xiong, J.; Yuan, C.; Semin, S.; Rasing, T.; Bu, X. H. Halide Perovskites for Nonlinear Optics. *Adv. Mater.* **2020**, *32*, 1806736.
- (46) Feng, X.; Sun, Z.; Pei, K.; Han, W.; Wang, F.; Luo, P.; Su, J.; Zuo, N.; Liu, G.; Li, H.; Zhai, T. 2D Inorganic Bimolecular Crystals with Strong In-Plane Anisotropy for Second-Order Nonlinear Optics. *Adv. Mater.* **2020**, *32*, 2003146.
- (47) Pramanik, A.; Gates, K.; Gao, Y.; Begum, S.; Ray, P. C. Several Orders-of-Magnitude Enhancement of Multiphoton Absorption Property for CsPbX3 Perovskite Quantum Dots by Manipulating Halide Stoichiometry. *J. Phys. Chem. C* **2019**, *123*, 5150–5156.
- (48) Wei, W.-J.; Jiang, X.-X.; Dong, L.-Y.; Liu, W.-W.; Han, X.-B.; Qin, Y.; Li, K.; Li, W.; Lin, Z.-S.; Bu, X.-H.; Lu, P.-X. Regulating Second-Harmonic Generation by van der Waals Interactions in Two-dimensional Lead Halide Perovskite Nanosheets. *J. Am. Chem. Soc.* **2019**, *141* (23), 9134–9139.
- (49) Li, L.; Shang, X.; Wang, S.; Dong, N.; Ji, C.; Chen, X.; Zhao, S.; Wang, J.; Sun, Z.; Hong, M.; Luo, J. Bilayered Hybrid Perovskite Ferroelectric with Giant Two-Photon Absorption. *J. Am. Chem. Soc.* **2018**, *140*, 6806–6809.
- (50) He, T.; Li, J.; Qiu, X.; Xiao, S.; Yin, C.; Lin, X. Highly Enhanced Normalized-Volume Multiphoton Absorption in CsPbBr3 2D Nanoplates. *Adv. Opt. Mater.* **2018**, *6*, 1800843.

- (51) Li, J.; Jing, Q.; Xiao, S.; Gao, Y.; Wang, Y.; Zhang, W.; Sun, X. W.; Wang, K.; He, T. Spectral Dynamics and Multiphoton Absorption Properties of All-Inorganic Perovskite Nanorods. *J. Phys. Chem. Lett.* **2020**, *11*, 4817–4825.
- (52) Ketavath, R.; Katturi, N. K.; Ghugal, S. G.; Kolli, H. K.; Swetha, T.; Soma, V. R.; Murali, B. Deciphering the Ultrafast Nonlinear Optical Properties and Dynamics of Pristine and Ni-Doped CsPbBr3 Colloidal Two-Dimensional Nanocrystals. *J. Phys. Chem. Lett.* **2019**, 10 (18), 5577–5584.
- (53) Chen, W. Q.; Bhaumik, S.; Veldhuis, S. A.; Xing, G. C.; Xu, Q.; Gratzel, M.; Mhaisalkar, S.; Mathews, N.; Sum, T. C. Giant five-photon absorption from multidimensional core-shell halide perovskite colloidal nanocrystals. *Nat. Commun.* **2017**, *8*, 15198.
- (54) Nagamine, G.; Rocha, J. O.; Bonato, L. G.; Nogueira, A. F.; Zaharieva, Z.; Watt, A. A. R.; de Brito Cruz, C. H.; Padilha, L. A. Two-Photon Absorption and Two-Photon-Induced Gain in Perovskite Quantum Dots. J. Phys. Chem. Lett. 2018, 9, 3478–3484.
- (55) Ray, P. C. Size and Shape Dependent Second Order Nonlinear Optical Properties of Nanomaterials and their Application in Biological and Chemical Sensing. *Chem. Rev.* **2010**, *110*, 5332–5365.
- (56) Schermelleh, L.; Ferrand, A.; Eggeling, C.; Huser, T.; Sauer, M.; Biehlmaier, O.; Drummen, G. P. C. Super-Resolution Microscopy Demystified. *Nat. Cell Biol.* **2019**, *21*, 72–84.
- (57) Chen, G.; Roy, I.; Yang, C.; Prasad, P. N. Nanochemistry and Nanomedicine for Nanoparticle-based Diagnostics and Therapy. *Chem. Rev.* **2016**, *116* (5), 2826–2885.
- (58) Vangara, A.; Pramanik, A.; Gao, Y.; Gates, K.; Begum, S.; Chandra Ray, P. Fluorescence Resonance Energy Transfer Based Highly Efficient Theranostic Nanoplatform for Two-Photon Bioimaging and Two-Photon Excited Photodynamic Therapy of Multiple Drug Resistance Bacteria. ACS Appl. Bio Mater. 2018, 1, 298–309.
- (59) Sinha, S. S.; Jones, S.; Pramanik, A.; Ray, P. C. Nanoarchitecture Based SERS for Biomolecular Fingerprinting and Label-Free Disease Markers Diagnosis. *Acc. Chem. Res.* **2016**, 49, 2725–2735.
- (60) Sweet, C.; Pramanik, A.; Jones, S.; Ray, P. C. Two-Photon Fluorescent Molybdenum Disulfide Dots for Targeted Prostate Cancer Imaging in the Biological II Window. *ACS Omega* **2017**, *2*, 1826–1835.
- (61) Cui, J.; Jiang, R.; Guo, C.; Bai, X.; Xu, S.; Wang, L. Fluorine Grafted Cu7S4—Au Heterodimers for Multimodal Imaging Guided Photothermal Therapy with High Penetration Depth. *J. Am. Chem. Soc.* 2018, 140 (18), 5890–5894.
- (62) Foulkes, W. D.; Smith, I. E.; Reis-Filho, J. S. Triple-Negative Breast Cancer. N. Engl. J. Med. 2010, 363, 1938–1948.
- (63) Zardavas, D.; Irrthum, A.; Swanton, C.; Piccart, M. Clinical management of breast cancer heterogeneity. *Nat. Rev. Clin. Oncol.* **2015**, *12*, 381–394.
- (64) Sharma, A.; Lee, M. G.; Won, M.; Koo, S.; Arambula, J. F.; Sessler, J. L.; Chi, S. G.; Kim, J. S. Targeting Heterogeneous Tumors Using a Multifunctional Molecular Prodrug. *J. Am. Chem. Soc.* **2019**, 141 (39), 15611–15618.
- (65) Fan, Z.; Shelton, M.; Singh, A. K.; Senapati, D.; Khan, S. A.; Ray, P. C. Multifunctional Plasmonic Shell—Magnetic Core Nanoparticles for Targeted Diagnostics, Isolation, and Photothermal Destruction of Tumor Cells. *ACS Nano* **2012**, *6*, 1065–1073.
- (66) Lu, W.; Singh, A. K.; Khan, S. A.; Senapati, D.; Yu, H.; Ray, P. C. Gold Nano-Popcorn-Based Targeted Diagnosis, Nanotherapy Treatment, and In Situ Monitoring of Photothermal Destruction Response of Prostate Cancer Cells Using Using Surface-Enhanced Raman Spectroscopy. J. Am. Chem. Soc. 2010, 132, 18103–18114.
- (67) Austin, L. A.; Kang, B.; El-Sayed, M. A. A New Nanotechnology Technique for Determining Drug Efficacy Using Targeted Plasmonically Enhanced Single Cell Imaging Spectroscopy. *J. Am. Chem. Soc.* **2013**, 135 (12), 4688–4691.
- (68) Li, H.; Yao, Q.; Sun, W.; Shao, K.; Lu, Y.; Chung, J.; Kim, D.; Fan, J.; Long, S.; Du, J.; Li, Y.; Wang, J.; Yoon, J.; Peng, X. Aminopeptidase N Activatable Fluorescent Probe for Tracking

Metastatic Cancer and Image-Guided Surgery via in Situ Spraying. J. Am. Chem. Soc. 2020, 142 (13), 6381–638.

- (69) Krishnakanth, K. N.; Seth, S.; Samanta, A.; Rao, S. V. Broadband femtosecond nonlinear optical properties of CsPbBr3 perovskite nanocrystals. *Opt. Lett.* **2018**, *43*, 603.
- (70) Chen, J.; Zidek, K.; Chabera, P.; Liu, D.; Cheng, P.; Nuuttila, L.; Al-Marri, M. J.; Lehtivuori, H.; Messing, M. E.; Han, K.; Zheng, K.; Pullerits, T. Size- and wavelength-dependent two-photon absorptioncross-section of CsPbBr₃ perovskite quantum dots. *J. Phys. Chem. Lett.* **2017**, *8*, 2316–2321.
- (71) Szeremeta, J.; Antoniak, M. A.; Wawrzynczyk, D.; Nyk, M.; Samoc, M. The Two-Photon Absorption Cross-Section Studies of CsPbX3 (X = I, Br, Cl) Nanocrystals. *Nanomaterials* **2020**, *10*, 1054.